Robotic Follower System Using Bearing-Only Tracking with Directional Antennas

Byung-Cheol Min[1] and Eric T. Matson[1,2]

[1] Machine-to-Machine (M2M) Lab, Department of Computer and Information Technology, Purdue University, West Lafayette, IN 47907 USA
[2] Department of Computer Engineering, Dongguk University, Seoul 100-715, Republic of Korea
{minb,ematson}@purdue.edu

Abstract. This paper presents the development of a robotic follower system with the eventual goal of autonomous convoying to create end-to-end communication. The core of the system is a bearing-only tracking with directional antennas and an obstacle avoidance algorithm with sonar sensors. For bearing estimation with directional antennas, we employ a Weighted Centroid Algorithm (WCA), which is a method for active antenna tracking and Direction Of Arrival (DOA) estimation. We also discuss the use of sonar sensors that can detect objects, which could improve our robotic follower system in mobile robot navigation. Through extensive field experiments in different environments, we show feasibilities of our proposed system, allowing a follower robot to track a leader robot effectively in convoying fashion. We expect that our system can be applied in a variety of applications that need autonomous convoying.

1 Introduction

In a disaster area, where previously established networks are destroyed, autonomous mobile robots carrying wireless devices can be deployed to create end-to-end communication. In the event of an earthquake disaster, like Fukushima, Japan, rapid establishment of a wireless backbone is useful, because it would allow rescuers and first responders to communicate and to coordinate evacuation and search-and-rescue missions effectively.

Typically, there are two means to build an end-to-end communication link with mobile robots. The first way is realized by planning robots' final positions prior to deployment of robots [1]−[5]. This planning should be designed for optimizing the communication link, and thus this approach is suitable for static environment rather than dynamic environments. Also, this is useful for cases where a rapid establishment of the network is required, because this way does not require a search task.

The second way is realized by deploying a team of leader-follower robots in convoying fashion [6]−[8]. The overview of this way is depicted in Fig. 1. In this way, multiple robots can be used, and only the leader requires navigation capabilities to create the network while followers do not require any planning.

J.-H. Kim et al. (eds.), *Robot Intelligence Technology and Applications 2*,
Advances in Intelligent Systems and Computing 274,
DOI: 10.1007/978-3-319-05582-4_4,

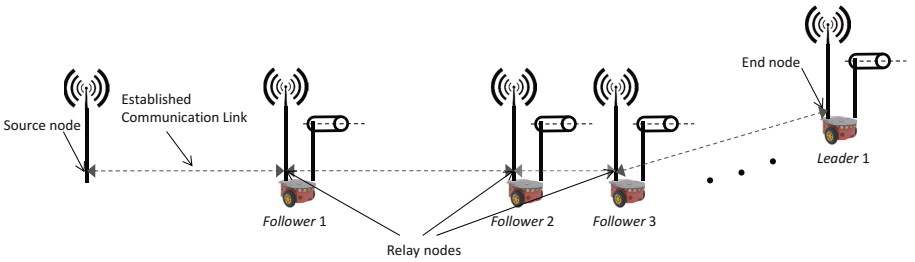

Fig. 1. The overview of a team of leader-follower robots to create end-to-end communication link

Alternatively, they need to follow the leader or the precedent robot. Therefore, this approach is suitable more for dynamic environments because this way is based on reactive approaches, not pre-planning approaches.

In this paper, we deal with the later way and propose a robotic follower system to create long-distance end-to-end communication. Leader-follower robots have been studied for a long time. Most of the work in this area focuses on control and algorithm aspects related to steering a follower robot so that it follows a leader robot. Other works study on sensors to enable follower behavior [11]. Typically, followers use one of the sensors such as a laser range finder, computer vision, GPS, Inertial Measurement Units (IMUs) to implement leader following strategies.

A vision based leader-follower system is the most common approach in convoying [9]. By estimating the leader's position form the sequence of video image, the follower can follow the leader. Although this approach shows powerful performances, there is a prerequisite condition that the sight of its leader should be guaranteed all the times in their system. Since the sight of its leaser is often lost (e.g., when the follower moves down the slope, the leader turns sharply, or objects lie between them), alternative ways to compensate it have to be incorporated. Also, it has been shown that identifying its leader among other possible objects is not easy such as obstacles and robots.

Other ways employ GPS or IMU to estimate the leader's position and heading [10][11]. During motion, the leader produces absolute way points, which are then followed by the follower. Because of the absolute position provided by GPS, position errors can be bounded and their leader-follower team can travel together by sharing the information. As this approach does not require line-of-light at all, it is known to be a good alternative way to use a vision-based follower system. However, outage of GPS signal due to limited places may result in position errors, finally causing the system to fail. Once the failure in communication takes place, the follower may not be able to track the leader.

In our system, we introduce directional antennas as a directional finder for the robotic follower system. For example, if there are two robots − one is a leader and the other is a follower − they are all equipped with a network device with

antennas and wirelessly connected to each other. More specifically, the leader is equipped with an omni-directional antenna and the follower has a directional antenna (this configuration will be explained later in detail). The follower estimates a bearing from the transmitter at the leader using the directional antenna and follows it with the estimated bearing.

Directional antennas have several advantages. First, they are easy to obtain and are affordable as compared to other sensory devices such a laser range finder and a vision system, they can be used in both indoor and outdoor environments as directional sensors, and they can also detect some objects [12]−[14]. Moreover, in contrast to the vision based leader-follower system, a directional antennas-based follower system can cope with cases where the sight of its leader is lost.

Although directional antennas have many advantages, it remains a challenge to increase their accuracy enough to use them as typical sensory devices, similar to laser or ultrasonic sensors in the field of mobile robotics. One common type of directional antenna (the type used in this study) has a beam width that is conical in shape [15]. This broad beam width allows directional antennas to measure a wide area; however, it also yields a coarser measurement resolution than that of the non-expanding beamwidth generated by a laser. In addition, because of the presence of walls and other objects that act as reflectors or scatters, the signals received by a directional antenna can consist of multiple copies of the transmitted signal that arrive via different paths. This effect gives rise to varying levels of received power, represented as sensor noise or uncertainty. Because the magnitude of this sensor noise is much larger than typical noise in other types of sensors, it may hinder directional antennas from being used as sensory devices. This necessitates some filtering of the received signal to remove such interference.

In this paper, we use a Direction Of Arrival (DOA) estimation technique for bearing estimation that is called the Weighted Centroid Algorithm (WCA) and is a type of weighted centroid approach. Weighted centroid approaches have been adopted by several research groups [16]−[19]. The previous studies used the "distance" as the weighting factor, through power measured from multiple anchor nodes. In [20], we examined the directionality of the radiation pattern with a stand-alone directional antenna for DOA estimation. As the basic concept of using weights to obtain the centroid of a data set is similar to the previous studies, we recommend referring to the papers referenced above for a more detailed explanation of the concept of weighted centroid approaches.

2 Follower Robotic System

In this paper, we adopt the strategy for deploying mobile relay nodes that was introduced in [6], in order to create long-distance end-to-end communication.

The overview of the strategy was depicted in Fig. 1. Multiple robots can be used in this system with the following rule − one robot should be a leader to act as an end node, and others should be followers to act as relay nodes connecting the wireless source node to the end node. They are linked sequentially with a wireless device. Then, all followers follow the leader in convoying fashion.

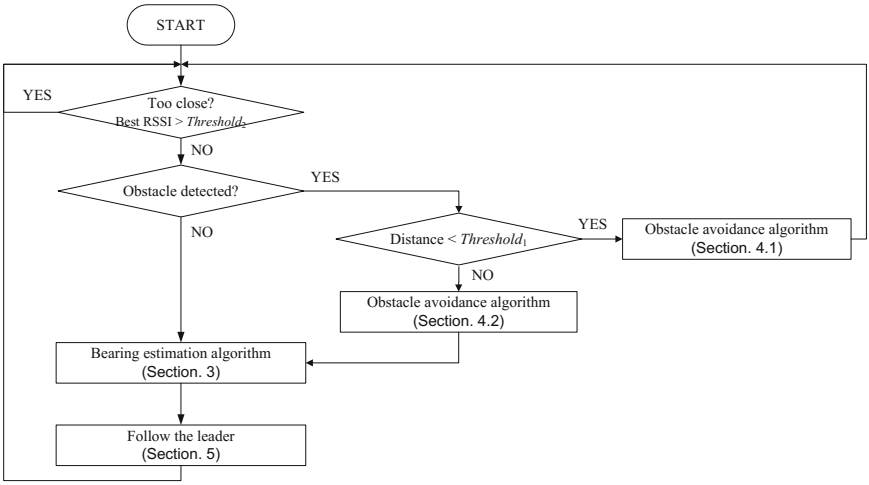

Fig. 2. A flow chart of the follower robotic system

When the link between the source node and the last follower (e.g., *Follower* 1 in Fig. 1) in the convoy is about to disconnect, that follower stops, and the rest of the convoy continues on. After that, when the link between the now stationary relay (*Follower* 1) and the last follower (*Follower* 2) in the remaining convoy is about to disconnect, that follower also stops and becomes a stationary relay. The process continues until all followers have been deployed.

The leader can be programmed to reach the goal position autonomously, but we control it manually through a remote control, in order to focus on the follower robotic system in this research. Alternatively, follower robots are autonomous to follow the leader. For follower robots to be autonomous, the follower robotic system runs with the steps, depicted in Fig. 2.

As shown in Fig. 2, the follower robot is composed mainly of two algorithms – a bearing estimation algorithm and an obstacle avoidance algorithm. The bearing estimation algorithm allows a follower robot to track the leader. We will detail this algorithm in Section 3. The obstacle avoidance algorithm allows the follower robot to avoid the obstacle between itself and the leader. For the obstacle avoidance algorithm, we employ two different ways, depending on a distance between the object to the follower robot. First, if the distance is too close (i.e., when measured distance is smaller than the pre-defined threshold), obstacle avoidance becomes a top priority, i.e., the robot stops following the leader and avoids the obstacle and tries to be in a safe place from any crash. For this way, we develop a simple obstacle avoidance algorithm and will detail it in Section 4.1. Second, if the distance is not close, but an object on the path is detected, we employ both bearing estimation algorithm and obstacle avoidance algorithm at the same time, i.e., the robot keeps following the leader while avoiding the object. For this later way, we introduce a penalty function and will detail it in Section 4.2.

3 Weighted Centroid Algorithm

In this section, we briefly describe the WCA, introduced in [20], for bearing estimation of the follower robot[1]. In Fig. 3, the receiver for bearing estimation attached to the follower is a directional antenna that can rotate horizontally by a servo motor, and the transmitter attached to the leader is a stationary omni-directional antenna, which is installed perpendicular to the ground. The omni-directional antenna on both sides is the real one for data transmission in end-to-end communication (not covered in this paper), so it is wirelessly paired together. Fig. 4 shows defined parameters for bearing estimation with a directional antenna, and detailed parameters are described in Table 1. For the interval angle θ^t, it is assumed that this angle can be computed by dividing the interesting range by the total number of measurements N_t.

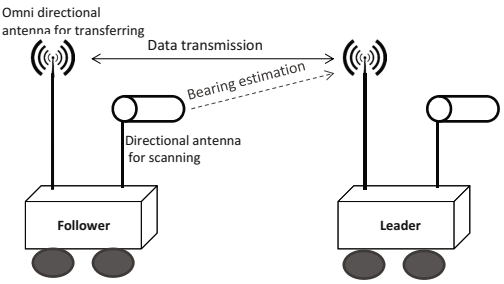

Fig. 3. The directional sensing model for leader-follower robotic system

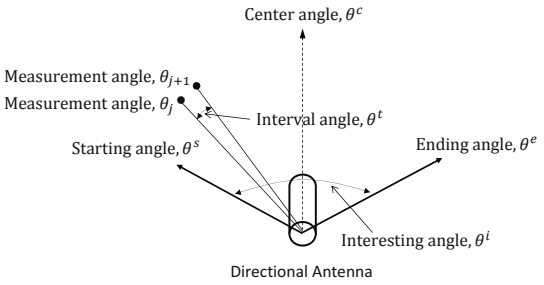

Fig. 4. Defined parameters for bearing estimation with a directional antenna, when scanning clockwise

[1] In [20], we used the term "DOA estimation" to represent bearing estimation that we use in this paper. Compared to the previous paper, this paper develops a considerably more comprehensive analysis on WCA.

Table 1. Setting of parameters

Variables	Description
θ^i	Interesting range where a scanning task performs, defined at the center of the antenna's body
θ^s	Starting angle where to start the range
θ^e	Ending angle where to end the range, going either clockwise or counter-clockwise from the starting angle in turn
θ^c	Center angle between the staring angle and the ending angle (at the beginning of scanning, the center angle is the front of the device)
θ^t	Interval angle of measurement
θ^j	Measurement angle, where j is the index of the measurement such that $j \in \{1, 2, \ldots, N_t\}$
N_t	Total number of measurements while scanning from the starting angle to the ending angle
$RSSI_j$	The measured RSSI at the jth measurement

Fig. 5 shows an example of measured RSSI (Radio Signal Strength Index) from an experiment that was conducted indoors, with a rotary directional antenna, showing the parameters in Table 1. In this figure, it is shown that $\theta^i = 180°$, $\theta^s = -90°$, $\theta^e = 90°$, $N_t = 13$, and therefore $\theta^t = 10°$.

In the first step of the WCA, a single rotary directional antenna measures the signal strength by rotating from θ^s to θ^e and produces a set of $RSSI_j$, as shown in Fig. 5. Here, θ^s and θ^e are determined by the center angle θ^c that is set to be aligned exactly on the previously calculated bearing to prevent the estimation from approaching the end where an actual bearing dwells [20].

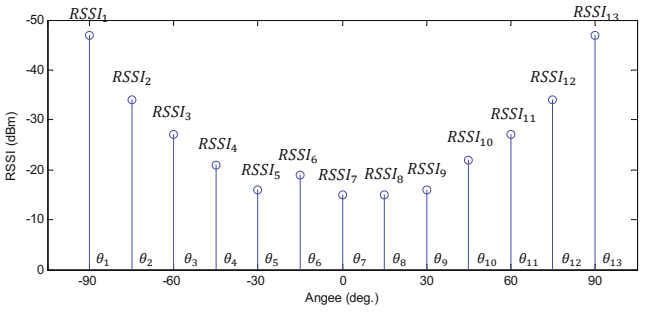

Fig. 5. An example of measured signal strength with a rotary directional antenna. The horizontal axis is the measurement angle and the vertical is the measured signal strength.

In the second step, a weight is computed by the measured signal strengths at θ_j using the following expression

$$w_j \ = 10^{\left(\frac{RSSI_j}{\gamma_1}\right)}. \tag{1}$$

where γ_1 is a positive gain that should be appropriately determined in every application scenario so that stronger signal strengths are more weighted than weaker signal strengths. Then, the bearing can be estimated by means of weighted centroid approaches as follows,

$$\widetilde{\Theta} = \frac{\sum_{j=1}^{N_t} w_j \theta_j}{\sum_{j=1}^{N_t} w_j} \tag{2}$$

If we use the measured RSSI shown in Fig. 5 again and depict all variables used in Eq. (2) in polar coordinates, it should look like Fig. 6. Here, γ_1 was set to 10, the estimated bearing $\widetilde{\Theta}$ using the WCA was depicted with a symbol "★" (See nearby 0° on angle-axis between -20 dBm and -30 dBm) in a polar coordinate, and the actual angle was depicted with a symbol "■".

The variance of the estimated bearing $\widetilde{\Theta}$ can be derived as follows. First, let the uncorrelated random variable X_j be a function of $\overline{p_{\mathrm{R}j}}$ multiplied by θ_j, where $\overline{p_{\mathrm{R}j}}$ is a normalized signal strength

$$\overline{p_{\mathrm{R}j}} = p_{\mathrm{R}_j} \frac{N_t}{\sum_{j=1}^{N_t} p_{\mathrm{R}_j}}. \tag{3}$$

In [19], the authors showed that random variables follow a Gaussian (Normal) distribution, with a mean μ_j and variation ${\sigma_j}^2$ as follows,

$$X_j \sim N\left(\mu_j, {\sigma_j}^2\right), \tag{4}$$

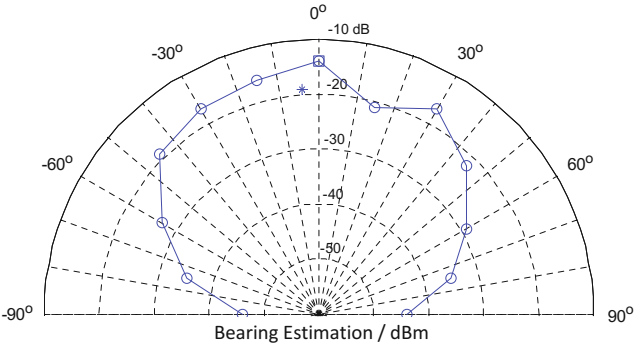

Fig. 6. Weighted Centroid Algorithm(WCA) in a polar coordinate frame

where ${\sigma_j}^2$ is the variation of received signal strength, represented as sensor noise or uncertainty, as mentioned in Section 1. Then, the mean of the random variables can be obtained as follows,

$$\overline{X} = \frac{1}{N_t}\sum_{j=1}^{N_t}\mu_j = \frac{1}{N_t}\sum_{j=1}^{N_t}\overline{p_{\mathrm{R}j}}\theta_j \tag{5}$$

and the variation is computed as

$$V\left(\overline{X}\right) = \frac{1}{{N_t}^2}\sum_{j=1}^{N_t}{\sigma_j}^2. \tag{6}$$

Consequently, when the variations of all observations are almost equal, ${\sigma_j}^2 \approx d$, we have $V\left(\overline{X}\right) \approx d/N_t$, which is related to the central limit theorem [21]. It is clearly shown that, as the sample number N_t increases, the variance $V\left(\overline{X}\right)$ decreases. This also verifies that, as we calculate the bearing based on multiple sampled data, the variation of bearing can be smaller in proportion to the sample number. In fact, the authors in [22]−[24] conducted multiple measurements from multiple devices, or from a long period, to have more sample data, and could produce a better estimation. However, because of the multiple measurements, it was very slow and computationally expensive to process their estimation methods. As shown in the equations derived in this section, the WCA only requires the summation and multiplication of data. Not only is the WCA computationally effective, but it estimates the bearing very accurately.

4 Obstacle Avoidance Algorithm

With the bearing estimation algorithm presented in the previous section, the follower can track the leader. However, if there is a static or dynamic obstacle between the two robots, the follower should avoid it first and continue following the leader. Therefore, a decent obstacle avoidance algorithm is necessary for a successful follower.

For this research, we use P3AT which is a mobile robot research platform available from Adept MobileRobots, Inc. [7]. There are eight sonar sensors attached to the front of the P3AT that can detect an object in front of the robot and measure the distance between the object and the robot. For an obstacle avoidance algorithm, we utilize these sensors.

We define in this paper that the follower may face with three different situations in terms of an obstacle − one is when the robot is free to obstacles so it can keep following the leader, the second is when the obstacle is too close (e.g., the distance between the robot and the obstacle is less than 1 meter), and the last is when the obstacle is detected, but not close.

4.1 When an Obstacle Is Too Close

In the second situation, since there is a high chance that a collision takes place, the robot should stop following the leader, and avoid the obstacle first with a

set of sonar sensors. Therefore, we have developed a simple obstacle avoidance algorithm that is also based on weighted centroid approach, calculating a direction guiding the robot to a safe region. This algorithm is mainly designed to avoid an obstacle, so it should be activated only when there is an object detected by a sonar sensor and its measured distance is shorter than a pre-determined threshold, $Threshold_1$.

In the first step of the algorithm, we compute a weight by the measured sonar distances using the following expression

$$w_k = 10^{\left(\frac{-Distance_k}{\gamma_2}\right)}, \tag{7}$$

where,

$$\begin{aligned} \gamma_2 &= \text{a positive gain} \\ Distance_k &= \text{a measured sonar distance in centimeters at } \phi_k, \\ &\quad \text{where } k \in \{1, 2, \ldots, N_s\} \\ N_s &= \text{the total number of sonar measurements.} \end{aligned}$$

As we defined in the previous section for bearing estimation, the center angle is the front of the device. P3AT has eight sonar sensors so each sensor has a field of view of approximately 25.7°, and the horizontal range of all sensors is from $-90°$ to $+90°$, implying that measurement angle $\phi_k \in \{-90°, -64.3°, \ldots, +90°\}$. Then, the direction $\widetilde{\Phi}$, guiding the robot to a safe region, can be estimated by means of weighted centroid approaches as follows,

$$\widetilde{\Phi} = \begin{cases} \hat{\Phi} + \left|\phi_1 + \phi_{N_s/2}\right| & \text{if } \hat{\Phi} \leq 0° \\ \hat{\Phi} - \left|\phi_1 + \phi_{N_s/2}\right| & \text{else} \end{cases} \tag{8}$$

where,

$$\hat{\Phi} = \frac{\sum_{k=1}^{N_s} w_k \phi_k}{\sum_{k=1}^{N_s} w_k}. \tag{9}$$

With Eqs. (7) - (9), the measured data with long distances to the object are depicted further from the center in the polar coordinate frame, and their angle values become more important to determine the weighted centroid. Conversely, shorter distances are rarely weighted because of the log scale. Therefore, the measured data with shorter distances are depicted closer to the center, and their angle values become less important. As a result, it can be said that Eqs. (8) and (9) calculates a reasonable direction by averaging the measured data with appropriate weighting.

4.2 When an Obstacle Is Detected, But Not Close

The algorithm for the second situation was developed to prevent the follower robot from colliding with objects. With this algorithm, we can prevent most of the crashes into obstacles. However, if we take only this situation into consideration, motions of the robot would become too large as approaching the obstacle.

For this reason, we have developed another algorithm for dealing with situations where an obstacle is detected, but not close. We believe that implementing this third algorithm remarkably helps reducing the chances that the robot faces with a dangerous situation from close objects like the second situation. Since the robot changes its heading in advance approaching the close objects, it will follow the leader more effectively and safely.

We utilize sonar sensors again for this algorithm in form of a penalty function. The basic concept of the penalty function is to integrate a sonar sensor measurement into an antenna measurement (i.e., if an object on the path is detected, then the function generates a pseudo RSSI measurement that is levied into a real RSSI measurement). This penalty function is activated only when there is an object detected by a sonar sensor, and its measured distance is longer than the pre-determined threshold for the second situation.

The steps for constructing and using the penalty function are as follows:

1. A function, sonar(ϕ), includes data of measured distances to an object, using the eight sonar sensors. This function can be expressed as

$$\text{sonar}(\phi_k), \text{where } k \in \{1, 2, \ldots, N_s\} \tag{10}$$

   where ϕ_k is a measurement angle, N_s is the total number of sonar measurements (eight for P3AT).
2. The sonar sensors and the directional antenna have different data set lengths ($N_s \neq N_t$). For instance, there would be eight sonar sensor measurements from the robot and 13 measurements from the directional antenna. When two measured data sets are combined into one data set, they must have the same length. Therefore, we expand the measured sonar sensor data, which is coarser, to have the same length as the data obtained from the antenna. This expansion is accomplished by linear interpolation that is obtained by passing a straight line between two adjacent data points, as follows,

$$\widetilde{\text{sonar}}(\phi) = \sum_{k=1}^{N_s} \text{sonar}(\phi_k) L_k(\phi) \tag{11}$$

   where for each $k = 1, 2, ..., N_s$,

$$L_k(\phi) = \prod_{i=1, i\neq k}^{N_s} \frac{(\phi - \phi_i)}{(\phi_k - \phi_i)} (1 \leq k \leq N_s). \tag{12}$$

   sonar(ϕ) is the exact function for which values are known only at a discrete set of data points, and the function $\widetilde{\text{sonar}}(\phi)$ is the interpolated approximation to sonar(ϕ).

   Using Eq. (11), the interpolated approximation of sonar(ϕ) can have the expanded range of $\widetilde{\text{sonar}}(\phi_j)$, where $j \in \{1, 2, \ldots, N_T\}$, meaning the sonar measurements could have the same data length as the antenna measurements. An example of this measurement expansion, using the linear interpolation, is depicted in Fig. 7. There are some gaps between the exact data and the approximated data, but they are negligible.

3. Using the expanded sonar sensor measurement, we generate penalty values (pseudo RSSI measurements), as follows,

$$\text{penalty}(\phi) = \alpha \exp(-\beta \widetilde{\text{sonar}}(\phi)), \tag{13}$$

where α and β are constants for regulating the level of the penalty function. The effects of different α values are depicted in Fig. 8. As shown in this figure, when α is higher, more penalty is levied. Here, as an example, we set $\alpha = 60$ and $\beta = 0.1$. Note that these two parameters should be carefully determined, depending on the material of the object that is detected by the sonar sensors. For example, if the material of the object is impenetrable with wireless signal, α could be set to a lower value. However, if the material of the object is penetrable, α should be set high enough for the obstacle to be recognized.

4. Using the penalty function in Eq. (13), The pseudo RSSI measurements $PRSSI_j$ is formed, and the real RSSI measurement using the antenna becomes,

$$NRSSI_j = RSSI_j + PRSSI_j \tag{14}$$

5. Returning to the original algorithm, $NRSSI_j$ is used instead of $RSSI_j$ as an input variable for WCA in Eq. (1).

The following two figures (Figs. 9 and 10) show the effectiveness of the penalty function. In these simulations, the leader was placed at the center of the map as a stationary transmitter. The first set was run without the penalty function (i.e. it depicts a case where there are only real RSSI measurements with a directional antenna). As shown in Fig. 9, the bearing was estimated to around 0° from the follower. Considering the follower depends on this estimated bearing for navigation, the follower would crash into the wall that lies between the transmitter and the follower's current position.

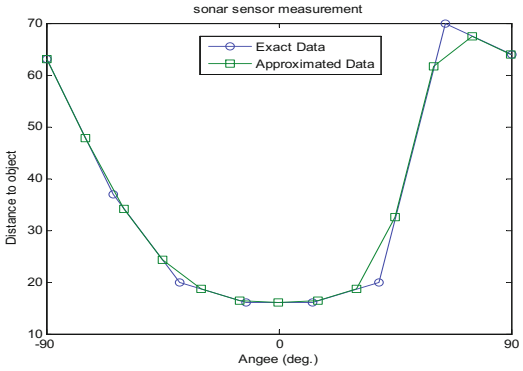

Fig. 7. Sonar measurements and their interpolation. The horizontal axis is the measurement angle and the vertical is the measured distance.

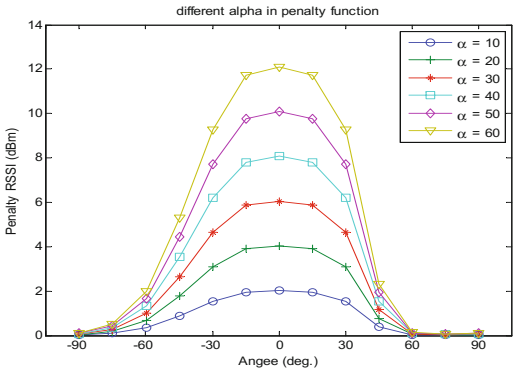

Fig. 8. Different α values in the penalty function. The horizontal axis is the measurement angle and the vertical is the pseudo signal strength, *PRSSI*.

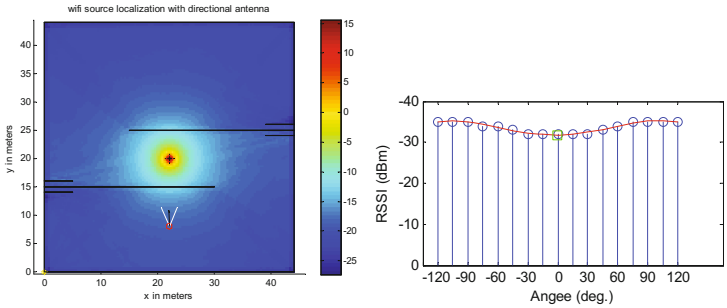

Fig. 9. Failure of bearing estimation with only real RSSI measurement. The left figure shows that the bearing was estimated to around 0°(See the black arrow), and the right figure shows the measured RSSI.

The second set was run with the penalty function (i.e. it depicts a case where there are real RSSI measurements, with pseudo RSSI measurements levied as a penalty). As shown in Fig. 10, the bearing was estimated to over +90°, pointing toward a roadway that allows the follower to come out to an open space. With the penalty function, even when the follower was located behind walls that could not be detected by a directional antenna, the bearing could be estimated to a safe and open region for robot navigation.

5 Mobile Robots Control

P3AT is a four-wheeled robot; however, two wheels on the same side are physically interconnected with a rubber belt. For the simple control of this robot for the follower robotic system, differential-drive mobile robots with characteristics of non-slipping and pure rolling are considered. The robot can be then controlled

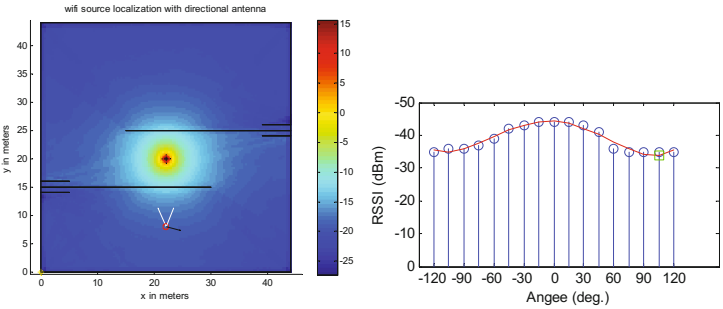

Fig. 10. Success in bearing estimation with real RSSI measurement, with penalty levied. The left figure shows that the bearing was estimated to over $+90^{\circ}$(see the black arrow), and the right figure shows the measured RSSI with pseudo RSSI added.

to move to any posture by adjusting the velocity of the left wheel V_L and the velocity of the right wheel V_R. V_L and V_R are calculated with either Eqs. (15) or (16), depending on the current situation of the robot.

$$\begin{aligned} V_L &= v_1 + k_{p1}\widetilde{\Theta} + k_{d1}(\widetilde{\Theta} - \widetilde{\Theta}^{t-1}) \\ V_R &= v_1 - k_{p1}\widetilde{\Theta} - k_{d1}(\widetilde{\Theta} - \widetilde{\Theta}^{t-1}) \end{aligned} \tag{15}$$

$$\begin{aligned} V_L &= v_2 + k_{p2}\widetilde{\Phi} + k_{d2}(\widetilde{\Phi} - \widetilde{\Phi}^{t-1}) \\ V_R &= v_2 - k_{p2}\widetilde{\Phi} - k_{d2}(\widetilde{\Phi} - \widetilde{\Phi}^{t-1}) \end{aligned} \tag{16}$$

If the follower lies in the first or third situation that we defined in the previous section, it runs with bearing estimation algorithm, activating Eq. (15) for the velocity control. If the follower lies in the second situation, it runs with the obstacle avoidance algorithm, activating Eq. (16) for the control. Therefore, in Eq. (15), $\widetilde{\Theta}$ is the current estimated bearing obtained by Eq. (2), $\widetilde{\Theta}^{t-1}$ is the old estimated bearing, k_{p1} and k_{d1} are positive gains, and v_1 is the background velocity of the robot, set to change according to a value of the best RSSI measurement from one scanning, i.e., v_1 is calculated by

$$v_1 = -\omega_1 RSSI^* - \omega_2, \tag{17}$$

where $RSSI^*$ indicates the best RSSI measurement in one scanning, ω_1 and ω_2 are should be set to a positive value and $w_2 \leq |w_1 \cdot RSSI^*|$ for v_1 to be a positive value.

In the same way, in Eq. (16), $\widetilde{\Phi}$ is the current estimated direction by Eq. (8), v_2 is a constant of the background velocity of the follower that we set to be low to avoid any dangerous situations (e.g., here we set v_2 to be 100, meaning 0.1 m/sec in a P3AT library), and k_{p2} and k_{d2} are positive gains.

For the robot stopping criteria, we use the following condition,

$$\begin{cases} V_L \text{ and } V_R = 0 & \text{if } RSSI^* \geq Threshold_2 \\ V_L \text{ and } V_R \text{ from Eqs.(15) or (16)} & \text{else.} \end{cases} \tag{18}$$

In Eq. (18), depending on a value of $Threshold_2$, we can differ how close the follower can get to the leader or prevent the follower from getting too close to the leader. Actually, the received power at the follower from the transmitter at the leader can be given by [25]

$$P_{dBm} = \underbrace{L_0 - 10n \cdot \log\left(\left\|x^t - x\right\|\right)}_{Fading} - \underbrace{f\left(x^t - x\right)}_{Shadowing} - \underbrace{\varepsilon}_{multipath}, \tag{19}$$

where L_0 is the measured power at 1m from the transmitter, n is the decay exponent, and x^t and x are the positions of the transmitter and receiver respectively. If terms of shadowing and multipath are very small compared to a term of fading, they can be negligible. Then, we can roughly calculate P_{dBm} by pre-obtaining L_0 and n with experiments. Therefore, we can select a proper value of $Threshold_2$ with Eq. (19) for a desired motion of our follower system. For example, we identified through experiments that -15 dBm of $Threshold_2$ keeps the follower away from the leader at intervals of 1 m in indoor environments and -20 dBm for outdoor environments.

6 Experiments

6.1 Preparation for Experiments

To test the proposed methods, we have developed a prototype of the leader-follower robotic system as shown in Fig. 11. The complete system mainly consists of a leader system and a follower system. The both systems can equip the same components, but we simplified the leader system for this research in order to focus on the follower system. The follower robotic system is made up of the P3AT mobile robot, a laptop, a yagi antenna, Wi-Fi USB adapter, and a pan-tilt servo device. And, for the ultimate goal of this research on end-to-end communication, we have installed two access points (AP) and a network switch. Later, by using a network switch in the communication system, we will be able to easily add additional network devices or laptops to the established communication link between the robots. The leader robotic system is equipped with almost same components as the follower has, but it does not have the yagi antenna and Wi-Fi USB adapter for this test.

For bearing estimation, we installed a small and light yagi antenna, manufactured by PCTEL. This device looks like a can and can be seen on the bottom of the system on the right side of Fig. 11 (a). This device has 10 dBi of gain, uses 2.4 GHz frequency range, and has 55° horizontal and vertical beamwidth at $1/2$ power. For the transmitter at the leader, requiring an omnidirectional antenna, we use a state of the art, low cost, high performance, and small wireless AP, PicoStation M2-HP, manufactured by Ubiquiti Networks Inc. This AP is equipped with a 5 dBi omnidirectional antenna, and supports passive Power over Ethernet (PoE), so it does not require an additional power code. Also, it runs with IEEE 802.11g protocol having an operating frequency of 2.4 GHz, and produces up to 28 dBm output power. As this device was designed to be deployed either indoor

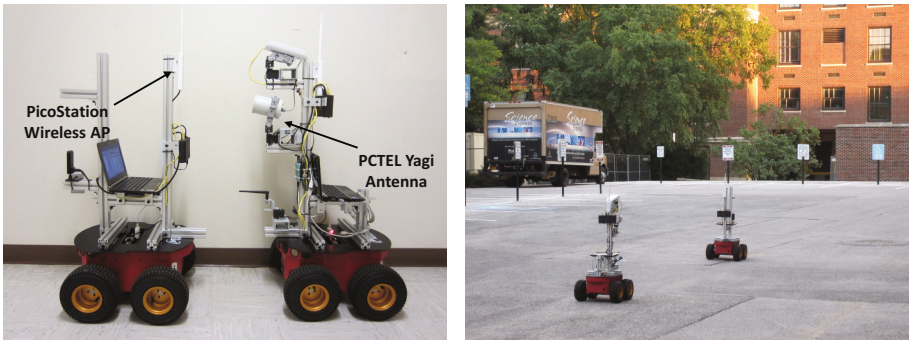

(a) leader-follower robotic system (b) field test

Fig. 11. Leader-follower robotic system composed of the follower system (left side on (a)) and the leader system (right side on (a))

or outdoor environments, it is ideal for applications requiring medium-range performance and a minimal installation footprint.

The laptop is connected by a serial connection to the P3AT, the pan-tilt device, and Alfa USB adapter. A pan-tilt device allows the directional antenna to be oriented in specific angle autonomously. In this paper, we employ a pan angle only as the directional antenna we chose for this project has about 55° beamwidth vertically, and therefore there are few cases that our robot is deployed out of the range. However, it should be noted that vertical beamwidth would also affect wireless communication in some cases.

For parameters needed in WCA and the obstacle avoidance algorithm, we set them as shown in Table 1. Due to the physical limitation of servo motors in our pan-tilt system, we set θ^i to be 180°. This setting results in the initial scan performed at $\theta^s = -90°$, $\theta^e = 90°$. N_t was approximately 25 for most of the tests. These settings were applied to all of the tests.

Table 2. Setting of parameters

Parameter	Value
θ^i	180°
$Threshold_1$	800 cm
$Threshold_2$	−25 dBm
γ_1, γ_2	10, 10
k_{p1}, k_{d1}	1.0, 0.3
k_{p2}, k_{d2}	1.2, 0.6
α, β	60, 0.1
w_1, w_2	10, 150

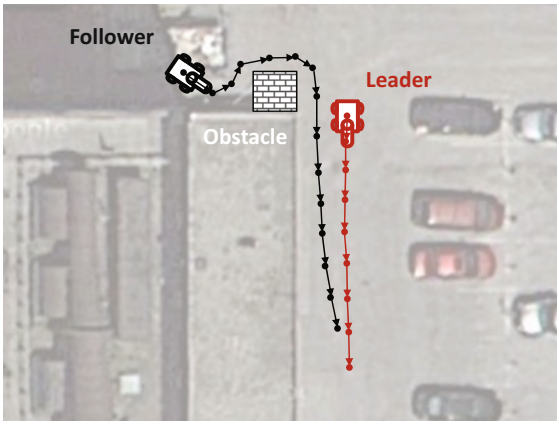

(a) traces of the two robots

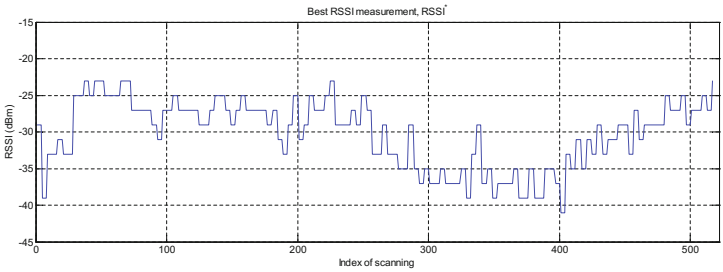

(b) history of the best RSSI

Fig. 12. Field test 1 (a video of this test is available at `http://web.ics.purdue.edu/~minb/rita2013.html`)

6.2 Experiments

In order to validate the proposed system, we conducted three different field tests. We chose ENAD parking lot at Purdue University for these tests, as shown in Figs. 12 to 14.

The first test was designed to analyze the performance of the obstacle avoidance algorithm. The leader was manually controlled so that it moves straight to about 15 m with a constant velocity at 0.2 m/sec. The follower was initially placed behind the building and the squared obstacle about the size of 0.5x0.5 m when viewed from above. In this planned situation, the follower should avoid the obstacle and the side of the building in order to follow the leader successfully. Otherwise, the follower fails to achieve its goal.

In Fig. 12 (a), the red lines indicate moved paths by the leader. The black lines indicate moved paths by the follower. These lines were drawn by referring to videos recorded during the test and odometer information from the robots. As shown in this figure, the follower could avoid the obstacle and the side of building without any contacts and follow the leader in the long run. Fig. 12 (b) shows

that a history of the measured best RSSI denoted with $RSSI^*$. As shown in the horizontal axis, approximately 520 times of scanning were performed during this test. During the first half of scanning, there were few decreases in measured RSSI as the leader and the follower were close to each other. While the leader bore off gradually and the follower focused on escaping from obstacles, measured RSSI became decreased up to about -40 dBm. However, as soon as the follower avoided the obstacles and became free, it resumed following the leader. After that, as shown in the end of the history in Fig. 12 (b), the measured RSSI reached to the pre-defined threshold, -25 dBm, making the follower stop with a close distance to the leader.

The second and third tests were designed to run for about 10 minutes each, in order to validate a robustness of the proposed system, including bearing estimation and the obstacle avoidance algorithm. The leader was manually controlled so that it moves along with pre-planned paths. The follower was initially placed just behind the leader.

Figure 13 shows the results of the second test. In Fig. 13 (a), the red lines show moved paths by the leader. The black lines show moved paths by the follower. As shown in this figure, the follower tracked way points that the leader produced relatively well during the entire test. It is shown that there are some noticeable gaps in the paths that two robots moved, but it results from the fact that the leader always moved ahead, resulting the follower changed its heading at a corner before it reaches the path that the leader moved. Figure 13 (b) shows a history of the best RSSI measurements. As shown in the horizontal axis, approximately 1500 times of scanning were performed during this test. Around the 1200th scanning, the leader was stopped intentionally, so the two robots got very closer to each other, resulting in about -20 dBm of the best RSSI. Since this value was lower than the threshold, the follower also stopped for a while. Because of this stop, the follower had to keep its pose pointing to a west direction. As the leader resumed moving to a south direction, the bearing between the two robots became almost a right angle, resulting in $-90°$ of bearing estimation from the follower. (see around the 1200th scanning in Figure 13 (c) that shows a history of the estimated bearing).

Figure 14 shows the results of the third test. This test includes multiple stops performed by the leader and very sharp paths requiring almost 180° turning for the follower to successfully follow the leader. Figure 14 (a) shows the tracked paths by the leader and the follower. As shown in this figure, the follower followed the leader well during the entire test. As the paths produced by the leader were relatively smooth until it rotated at the right top of the map, the difference in the paths the two robots moved was not shown unlike the previous test. There were two times of stop taken by the leader during the first half of the test. As shown in Fig. 14 (b) around the 300th and 500th scannings, the best RSSI reached the threshold accordingly, and therefore the follower stopped as well with a close distance to the leader. These behaviors validate that two robots in convoying performs successfully with the proposed system.

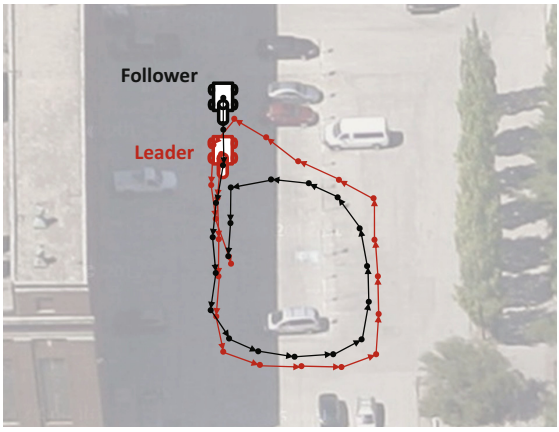

(a) traces of the two robots

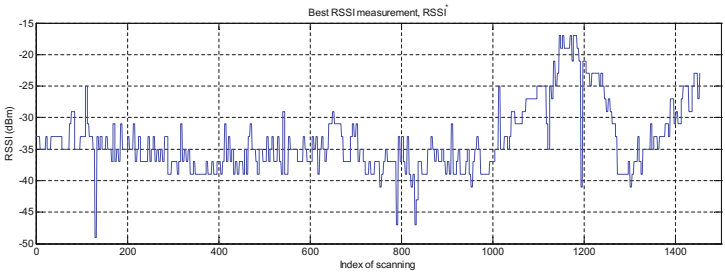

(b) history of the best RSSI

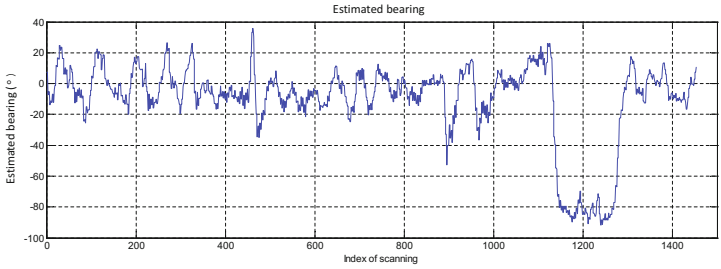

(c) history of the estimated bearing

Fig. 13. Field test 2 (a video of this test is available at `http://web.ics.purdue.edu/~minb/rita2013.html`)

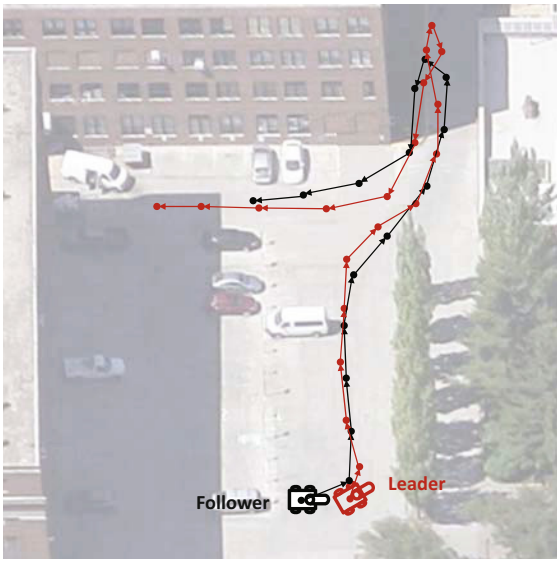

(a) traces of the two robots

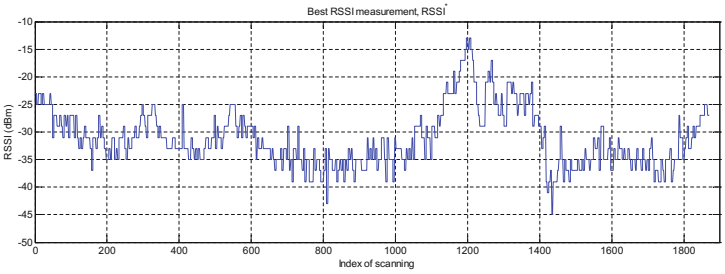

(b) history of the best RSSI

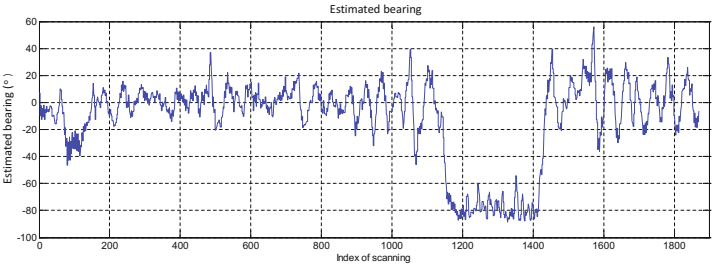

(c) history of the estimated bearing

Fig. 14. Field test 3 (a video of this test is available at `http://web.ics.purdue.edu/~minb/rita2013.html`)

From the right top of the map in Fig. 14 (a), one can see that the leader wheeled about to the other extreme. This was intended motion controlled by a human to see if the follower could follow the leader or not. As the leader turned to the opposite direction that the follower headed, the estimated bearing by the reader showed all the way to the left, meaning that the follower needs to change its heading to the left as well. However, since the measured RSSIs were lower than the threshold at that time, the follower had to stop for a while until the leader moved away from the follower (see around the 1200th scanning in Fig. 15 (b)). After the 1300th scanning, the best RSSI became higher than the threshold, and finally the follower turned sharply and resumed following the leader again.

7 Conclusion

We proposed a robotic follower system using directional antennas with the eventual goal of autonomous convoying to create end-to-end communication. With DOA estimation called the Weighted Centroid Algorithm, directional antennas could be utilized for guiding a follower robot to a leader robot. For mobile robot navigation, we developed a simple obstacle avoidance algorithm that is also based on weighted centroid approach, calculating a direction guiding the robot to a safe region. As a result, our system yielded very robust direction estimations in a constrained environment, specifically when the follower was placed in a region out of line of sight with the leader. Our future works will be devoted to increase the number of robots in convoying test, and discuss the use of this system in building long-distance end-to-end communication.

References

1. Bezzo, N., Fierro, R.: Tethering of mobile router networks. In: American Control Conference (ACC), pp. 6828–6833 (2010)
2. Pei, Y., Mutka, M.W.: Steiner traveler: Relay deployment for remote sensing in heterogeneous multi-robot exploration. In: 2012 IEEE International Conference on Robotics and Automation (ICRA), pp. 1551–1556 (2012)
3. Yan, Y., Mostofi, Y.: Robotic Router Formation in Realistic Communication Environments. IEEE Transactions on Robotics 28, 810–827 (2012)
4. Tekdas, O., Kumar, Y., Isler, V., Janardan, R.: Building a Communication Bridge With Mobile Hubs. IEEE Transactions on Automation Science and Engineering 9, 171–176 (2012)
5. Dixon, C., Frew, E.W.: Maintaining Optimal Communication Chains in Robotic Sensor Networks using Mobility Control. Mobile. Netw. Appl. 14, 281–291 (2009)
6. Nguyen, H.G., Pezeshkian, N., Raymond, M., Gupta, A., Spector, J.M.: Autonomous Communication Relays for Tactical Robots. In: Proceedings of the International Conference on Advanced Robotics (ICAR) (2003)

7. Nguyen, C.Q., Min, B.-C., Matson, E.T., Smith, A.H., Dietz, J.E., Kim, D.: Using Mobile Robots to Establish Mobile Wireless Mesh Networks and Increase Network Throughput. International Journal of Distributed Sensor Networks 2012, Article ID 614532, 1–13 (2012)
8. Tuna, G., Gungor, V.C., Gulez, K.: An autonomous wireless sensor network deployment system using mobile robots for human existence detection in case of disasters. Ad Hoc Networks (2012)
9. Giesbrecht, J.L., Goi, H.K., Barfoot, T.D., Francis, B.A.: A vision-based robotic follower vehicle. In: Proc. of the SPIE Defence, Security and Sensing, vol. 7332, pp. 14–17 (2009)
10. Hogg, R., Rankin, A.L., McHenry, M.C., Helmick, D., Bergh, C., Roumeliotis, S.I., Matthies, L.H.: Sensors and algorithms for small robot leader/follower behavior. In: Proc. of the 15th SPIE AeroSense Symposium (2001)
11. Borenstein, J., Thomas, D., Sights, B., Ojeda, L., Bankole, P., Fellars, D.: Human leader and robot follower team: correcting leader's position from follower's heading. In: Proc. of the SPIE Defence, Security and Sensing, vol. 7692 (2010)
12. Tokekar, P., Vander Hook, J., Isler, V.: Active target localization for bearing based robotic telemetry. In: 2011 IEEE/RSJ International Conference on Intelligent Robots and Systems (IROS), pp. 488–493 (2011)
13. Kim, M., Chong, N.Y.: RFID-based mobile robot guidance to a stationary target. Mechatronics 17, 217–229 (2007)
14. Kim, M., Chong, N.Y.: Direction Sensing RFID Reader for Mobile Robot Navigation. IEEE Transactions on Automation Science and Engineering 6, 44–54 (2008)
15. Graefenstein, J., Albert, A., Biber, P., Schilling, A.: Wireless node localization based on RSSI using a rotating antenna on a mobile robot. In: 6th Workshop on Positioning, Navigation and Communication (WPNC 2009), pp. 253–259 (2009)
16. Blumenthal, J., Grossmann, R., Golatowski, F., Timmermann, D.: Weighted Centroid Localization in Zigbee-based Sensor Networks. In: IEEE International Symposium on Intelligent Signal Processing (WISP 2007), pp. 1–6 (2007)
17. Behnke, R., Salzmann, J., Grossmann, R., Lieckfeldt, D., Timmermann, D., Thurow, K.: Strategies to overcome border area effects of coarse grained localization. In: 6th Workshop on Positioning, Navigation and Communication (WPNC 2009), pp. 95–102 (2009)
18. Pivato, P., Palopoli, L., Petri, D.: Accuracy of RSS-Based Centroid Localization Algorithms in an Indoor Environment. IEEE Transactions on Instrumentation and Measurement 60, 3451–3460 (2011)
19. Wang, J., Urriza, P., Han, Y., Cabric, D.: Weighted Centroid Localization Algorithm: Theoretical Analysis and Distributed Implementation. IEEE Transactions on Wireless Communications 10, 3403–3413 (2011)
20. Min, B.-C., Matson, E.T., Khaday, B.: Design of a Networked Robotic System Capable of Enhancing Wireless Communication Capabilities. In: 11th IEEE International Symposium on Safety, Security, and Rescue Robotics (SSRR 2013), Sweden, October 21-26 (2013)
21. Montgomery, D.C., Runger, G.C., Hubele, N.F.: Engineering Statistics, Student Study edn. John Wiley & Sons (2009)

22. Yang, C.-L., Bagchi, S., Chappell, W.J.: Topology Insensitive Location Determination Using Independent Estimates Through Semi-Directional Antennas. IEEE Transactions on Antennas and Propagation 54, 3458–3472 (2006)
23. Malajner, M., Planinsic, P., Gleich, D.: Angle of Arrival Estimation Using RSSI and Omnidirectional Rotatable Antennas. IEEE Sensors Journal 12, 1950–1957 (2011)
24. Sun, Y., Xiao, J., Li, X., Cabrera-Mora, F.: Adaptive Source Localization by a Mobile Robot Using Signal Power Gradient in Sensor Networks. In: IEEE Global Telecommunications Conference (IEEE GLOBECOM 2008), pp. 1–5 (2008)
25. Fink, J., Kumar, V.: Online methods for radio signal mapping with mobile robots. In: 2010 IEEE International Conference on Robotics and Automation (ICRA), pp. 1940–1945 (2010)